NANOSYSTEMS:
PHYSICS, CHEMISTRY, MATHEMATICS

Original article

Rezvanova A.E., et al. *Nanosystems: Phys. Chem. Math.*, 2023, **14** (5), 530–538.
http://nanojournal.ifmo.ru
DOI 10.17586/2220-8054-2023-14-5-530-538

Composite hydroxyapatite-multi-walled carbon nanotubes: study of porosity by terahertz time domain spectroscopy

Anastasiya E. Rezvanova[1,a], Boris S. Kudryashov[1,b], Alexander N. Ponomarev[1,c], Anastasiya I. Knyazkova[2,d], Victor V. Nikolaev[2,e], Yuri V. Kistenev[2,f]

[1]Institute of Strength Physics and Materials Science of the Siberian Branch of the Russian Academy of Sciences, Tomsk, Russia

[2]Tomsk State University, the Faculty of Physics, Tomsk, Russia

[a]ranast@ispms.ru, [b]bsk3@ispms.ru, [c]alex@ispms.ru, [d]a_knyazkova@bk.ru, [e]vik-nikol@bk.ru, [f]yuk@iao.ru

Corresponding author: A.E. Rezvanova, ranast@ispms.ru; B.S. Kudryashov, bsk3@ispms.ru

PACS 42.25.Gy, 42.25.-p, 33.60.Fy, 07.79.Fc

ABSTRACT Optical properties of a ceramic biocomposite material based on hydroxyapatite (HA) with the additives up to 0.5 wt.% of multi-walled carbon nanotubes (MWCNTs) have been studied by terahertz time-domain spectroscopy in the frequency range 0.25 – 1.1 THz. It was found that the refractive index of the composite varies between 2.6 and 2.8 depending on the porosity of the material. The absorption coefficient decreases with increasing of MWCNTs concentration in the ceramic biocomposite. The values of the refractive index and the absorption coefficient of our ceramics close to those for cortical bone, dentine and enamel. The absorption curves show frequency peaks whose positions correspond to the macrocrystallite sizes. The size of macrocrystallites decreases with increasing concentration of MWCNTs, which leads to an increase in microhardness according to the Hall–Petch equation. The time delay of the terahertz signal through the sample increases for higher concentration of MWCNTs. This indicates that nanotubes embedded into the HA matrix fill the pores and decrease the area of the pore space, which increases the density of the ceramic composite and decreases its porosity.

KEYWORDS ceramic composite, hydroxyapatite, multi-walled carbon nanotubes, terahertz spectroscopy, porosity

ACKNOWLEDGEMENTS The work by Rezvanova, Ponomarev, and Kudryashov was performed within the Government Statement of Work for the ISPMS SB RAS, project FWRW-2022-0002 and FWRW-2021-0007. The research by Knyazkova, Nikolaev, and Kistenev was supported by the grant under RF Government Decree No. 220 dated 09 April 2010 (Agreement No. 075-15-2021-615 of 04 June 2021). The authors are grateful to A. A. Neiman from the Nanotekh Regional Core Facility Centre of the Institute of Strength Physics and Materials Science SB RAS for his help with SEM images.

FOR CITATION Rezvanova A.E., Kudryashov B.S., Ponomarev A.N., Knyazkova A.I., Nikolaev V.V., Kistenev Yu.V. Composite hydroxyapatite-multi-walled carbon nanotubes: study of porosity by terahertz time domain spectroscopy. *Nanosystems: Phys. Chem. Math.*, 2023, **14** (5), 530–538.

1. Introduction

Calcium phosphate biomaterials, such as hydroxyapatite (HA), have excellent biocompatibility, bioactivity, osteoconductivity, and long degradation time. It makes them applicable in producing bone implants for orthopedic and dental medicine [1, 2]. Porosity is one of the important properties of biomedical materials, which is defined as the ratio of the void volume to the total volume of a porous material. The influence of porosity on the mechanical properties from one side and degradation, biocompatibility, and osteogenesis of the bioceramic scaffold, from the other side, should be taken into account in the design of such implants [3]. Porosity plays a significant role in bone tissue regeneration [4], crack propagation and fracture toughness of HA ceramics [5]. The porosity of HA ceramics depends on the amount of the multi-walled carbon nanotubes (MWCNTs) additives [5, 6]. MWCNTs additives increase the density of HA-MWCNTs composites by activating the sintering process in ceramics [2, 6].

The porosity of ceramic materials, the total porosity of open and closed pores can be measured by destructive and non-destructive methods [7–11]. Destructive methods include liquid pycnometry [7] and mercury porosimetry [8] that based on invasive analysis. These methods have several disadvantages including the destruction of a sample, losing mechanical and other properties.

The most common nondestructive methods are small-angle neutron scattering [9], transmission electron microscopy [10], the nuclear magnetic resonance method [11], etc. These methods allow one to carry out a noncontact,

noninvasive and fast analysis of the material porosity. The method of terahertz time-domain spectroscopy (THz-TDS) can be also used for this purpose. It holds certain advantages. The THz method [12] consists in recording the temporal shape of a terahertz electric field pulse after passing through the material matrix and analyzing it using the fast Fourier transform. Terahertz electromagnetic waves can penetrate through various materials, such as biomaterials, including polymers and ceramic materials, thereby providing their spectroscopic data [13]. The photon energy of THz waves is several orders of magnitude lower than the quantum energy of the X-ray wave. That is why the THz wave is a more efficient tool for nondestructive noncontact investigation [14, 15].

The analysis of the behavior of a THz pulse propagating through a sample makes it possible to determine such optical properties as absorption coefficient, refractive index, and THz pulse propagation time delay, which are used to estimate the material porosity [13]. The nonionizing radiation between 0.5 and 1.5 THz enables safe investigation of optical properties of human tissues and tissue replacement materials [16]. THz-TDS was used for in vitro studies of refractive indices and absorption coefficients of the jawbone [12], tooth enamel [17], dentin [17], cortical bone [18] and femoral bone [19]. The refractive index of enamel is bigger than that of dentin, while absorption has a similar frequency dependence [17]. In [20] the possibility of using THz spectroscopy for diagnosing dental caries is observed. It was shown, that the attenuation of the THz signal during caries is significantly higher than the one for healthy teeth.

The aim of this work is to study the optical properties of a porous ceramic biocomposite material by noninvasive THz time-domain spectroscopy in the frequency range 0.25 – 1.1 THz. The studies were performed on HA-based ceramic samples with different concentrations of MWCNTs (up to 0.5 wt.%). Refractive index, absorption coefficient and time delay of the terahertz pulse propagation through the HA-MWCNTs ceramic composite material were determined.

2. Materials and methods

2.1. HA-MWCNTs composites

The object of terahertz (THz) studies is a ceramic composite material with the hydroxyapatite (HA) matrix. The additives of multi-walled carbon nanotubes (MWCNTs) are used for reinforcement and control of porosity of the HA material structure. The studies were carried out on three sample sets: the HA and HA with 0.1 and 0.5 wt.% MWCNTs additives.

Hydroxyapatite was synthesized from calcium carbonate and orthophosphoric acid: $5CaCO_3$+$3H_3PO_4$+$Ca_5(PO_4)_3OH$+$4H_2O$+$5CO_2$. The HA powder was calcinated at the temperature 850 °C for 1 h in wet atmosphere and then mixed with the MWCNTs powder [6, 21, 22]. MWCNTs with the mean diameter 18 nm were prepared using the chemical vapor deposition (CVD) method [23, 24] and characterized by the calorimetric, scanning electron microscopy (SEM), Energy Dispersive X-ray microanalysis (EDX), X-ray photoelectron spectroscopy (XPS), transmission electron microscope (TEM) and near edge X-ray absorption fine structure (NEXAFS) spectroscopy [25–27]. The MWCNTs powder contains a small amount of the Co/Fe catalyst (less than 0.3 wt.%) and has a high-quality surface with a small number of defects and other impurities.

Cylindrical samples were prepared under the pressure 120 MPa and subsequent annealing at the temperature 1100 °C in argon atmosphere for 1 hour [2,5]. The thickness and diameter of the ceramic samples are 3 ± 0.1 mm and 8 ± 0.05 mm, respectively. The porosity was calculated using the theoretical density 3.167 g/cm^3 of stoichiometric HA [5]. The density of samples is varied from 8 to 27.5 % by changing the concentration of nanotubes.

This is consistent with a decrease in porosity near 3 times for HA+0.5 wt.% MWCNTs in comparison to HA without MWCNTs additives, that was found by the Brunauer–Emmett–Teller (BET)-method [28]. MWCNTs in the composite fill the pores between the HA grains, according for SEM characterization [2, 28].

2.2. Sample characterization

NEXAFS spectra of HA and HA with the additives of the MWCNTs were measured at the RGL-PES station of the 3rd generation synchrotron radiation source BESSY II (Berlin, Germany) in high-vacuum conditions ($\sim 10^{-10}$ Torr). The samples were degassed in dynamic high-vacuum conditions for more than 12 hours. Leakage current mode of the Keithley picoammeter was used for obtaining the NEXAFS spectra. The depth of the NEXAFS analysis was 15 – 20 nm. The spectra were used to analyze the chemical state and the local atomic structure of carbon in the MWCNTs. The NEXAFS spectra were normalized to the recorded contemporaneously of primary flux from a gold covered grid. The energy resolution of the monochromator in the ranges of the carbon K-edge ($h\nu \sim 285$ eV) was equal to ~ 70 meV.

The SEM images of the samples were obtained and characterized by using Zeiss EVO-50 field emission SEM (Carl Zeiss SMT Ltd.) at the accelerating voltage of 15.0 kV.

Optical characteristics of HA-MWCNTs were analyzed using a T-SPEC spectrometer (EKSPLA, Estonia). It operates in the frequency range 0.25 – 1.3 THz in the transmission mode. Sketch of T-SPEC spectrometer [29] is shown in Fig. 1(a). It has 4 main components:

— femtosecond pulse laser in the near-infrared range;
— terahertz emitter (photoconductive antenna, i.e. an optically activated fast switch built into the antenna structure);
— delay mechanism between the pumping and probing beams;

— THz detector with time synchronization.

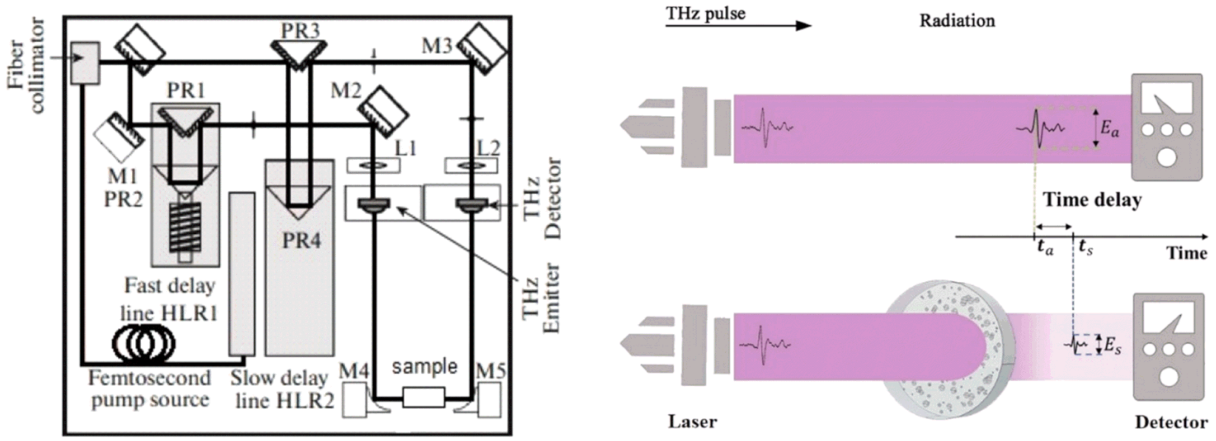

(a) (b)

FIG. 1. (a) T-SPEC Real-Time Terahertz Spectrometer: M1, M2, M3, M4, M5 – mirrors, L1, L2 – lenses, PR1, PR2, PR3, PR4 – prisms, HLR1 – fast delay line, HLR2 – slow delay line; (b) sketch of the terahertz pulse propagations through air and a sample

The femtosecond fiber laser is used at the pulse duration 10 – 150 fs, central wavelength 1050 ± 40 nm, pulse repetition rate 30 – 100 MHz, and power 100 mW. The laser output radiation is divided into two optical paths – the pumping and probing beams – by using the polarizing beam splitter (BS1). After the HLR1 delay line, the pumping beam is focused on the source of subpicosecond pulses of THz radiation (photoconductive antenna). The terahertz beam is focused on a sample spot using parabolic mirrors. The photoconductive output of the THz detector is proportional to the strength of the instantaneous electric field of the THz pulse generated during the ultrashort pumping pulse. Scanning with a fast delay line at the frequency 10 Hz forms the wave front of the electric field of THz radiation.

Sample response and a reference measurement are used to calculate the refractive index and absorption coefficient. The collected data then processed using the Fourier transform [30, 31]. In the transmission mode, the temporal response of the detector (time domain) is converted into the frequency characteristic of detector (frequency domain). If electric field strengths of the reference (in air medium without sample) and sample signals are denoted by $E_a(\omega)$ and $E_s(\omega)$, respectively, the ratio between the sample and reference pulses can be written as (1):

$$\frac{E_a\left(\omega\right)}{E_s\left(\omega\right)} = Ae^{i\Delta\varphi}, \tag{1}$$

where A is the magnitude of the ratio and $\Delta\varphi$ is the phase difference. It can also be written as (2):

$$\frac{E_s\left(\omega\right)}{E_a\left(\omega\right)} = T\left(\omega\right)e^{i\frac{\omega}{c}(\widehat{n_s}-1)d}, \tag{2}$$

where ω is the angular frequency, c is the speed of light, $T(\omega)$ is the Fresnel transmission coefficient, d is the sample thickness, and $\widehat{n_s}$ is the frequency-dependent complex refractive index of the sample. The value of $\widehat{n_s}$ is the sum of the two components: the refractive index $n_s(\omega)$ and the absorption (extinction) coefficient $k_s(\omega)$ (3):

$$\widehat{n_s}\left(\omega\right) = n_s\left(\omega\right) + k_s\left(\omega\right). \tag{3}$$

A sketch of the terahertz pulse propagations through the air and the ceramic sample during measurements is shown in Fig. 1(b).

The signal $E_a(\omega)$ propagates for time t_a during the measurements of a reference pulse in the absence of a sample. In the second measurement during the THz pulse propagates through the sample, the signal intensity decreases $E_s(\omega) < E_a(\omega)$ and the signal propagation time increases $t_s < t_a$, that lead to the time delay $\Delta t = t_a - t_s$ of the THz pulse propagation through a denser medium.

The refractive index n_s of the sample is obtained using the phase delay, according to Eq. (4):

$$n_s = 1 + \frac{c}{\omega d}\Delta\varphi. \tag{4}$$

The Fresnel transmission coefficient $T(\omega)$ is evaluated by using the calculated refractive index n_s. The absorption coefficient a_s is calculated by Eq. (5):

$$a_s = \frac{2\omega k_s}{c} = -\frac{2}{d}\ln\left(\frac{A}{T\left(\omega\right)}\right). \tag{5}$$

The sample is placed in the path of propagation of THz radiation in a special metal cell-holder. First, rough 2D scanning is performed over the entire surface of the sample (the scan area 3.6×3.6 mm and the vertical and horizontal scan step 0.25 mm). Then, the THz signal propagating through the center of the cell (the scan area 1.5×1.5 mm and the vertical and horizontal scan step 0.5 mm) is recorded, which makes it possible to avoid artifacts due to the metal cell-holder. Nine measurements were performed on each sample. The spectrum was averaged over 256-ps intervals to obtain a better signal-to-noise ratio.

Data are visualized using the TeraVil program for the T-SPEC spectrometer. Statistical analysis and data processing are carried out in Python 3.6 using libraries (numpy, scipy, matplotlib) and GNU Octave 6.4.0. free software.

3. Results and discussion

The density of the unoccupied states of carbon and the local atomic structure of HA-MWCNTs were investigated by the XANES method (see Fig. 2). The atomic and electronic structures of HA-MWCNTs depend on the concentration of MWCNTs. NEXAFS absorption spectra for the initial MWCNTs that used as the additives in the composite ceramics is shown in Fig. 2 for comparison [25]. For MWCNTs the structure of the π^*(C=C) resonance at the photon energy ~ 285 eV, σ (C=C) resonance at ~ 291 eV is observed [25]. For composites HA with MWCNTs observed the presence of the π^* (C=O) and σ^* (C–O) states that can indicate the possible oxidation of the MWCNTs from water produced during the dehydroxylation of HA. It is seen that with the increasing of the concentration of MWCNTs additives the intensity of π^* (C=C) and σ^*(C=C) chemical bonds decreases and at the same time the intensity with energy near 284 eV increase, that apparently related to the decomposition of MWCNTs and increasing the amount of amorphous carbon. Therefore, it is possible to assume that the presence of the MWCNTs leads to the activation of sintering processes of HA ceramics and increase of density. The partial carbonization of HA ceramics with the MWCNTs additives was indicated by the results of FT-IR studies [2]. With increasing of the amount of nanotubes in composite ceramics, the intensity of the carbonate stretching band of FT-IR spectra increases due to partial oxidation of the nanotubes and as a result more intensive carbonization of the A-type HA [2].

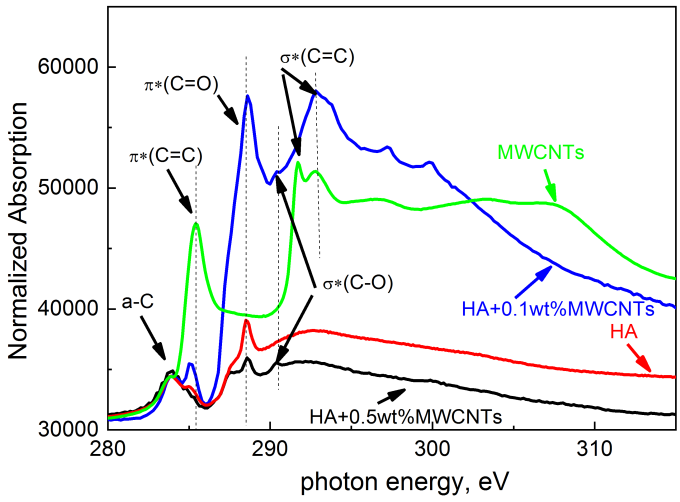

FIG. 2. XANES spectra of initial MWCNTs (green curve), HA (red curve), HA with 0.1 wt.% MWCNTs (blue curve) and HA with 0.5 wt.% MWCNTs (black curve)

The temporal wave forms of the field of the THz pulses transmitted through the air (reference) and composite HA ceramics and HA with the MWCNTs concentrations 0.1 and 0.5 wt.% were obtained by measurements of electric field strengths. The total number of such wave forms was 54. The dependencies for the electric field strength on the time of THz pulse propagation through the air and ceramics HA, HA+0.1 wt.% MWCNTs and HA+0.5 wt.% MWCNTs are shown in Fig. 3(a).

As it is seen in Fig. 3(a), the time delay appears between the THz pulse through the air (reference) and ceramic sample. The THz signal propagation time for the reference and the sample were measured by the THz detector with time synchronization, and the time delay of the pulse was determined as the difference between the main time peaks of the reference and the sample.

Figure 3(b) shows the linear dependence of the THz pulse time delay vs. the MWCNTs concentration and the porosity of the ceramic biocomposite. The time delay increases with a decreasing of the porosity [32, 33]. It is seen in the Fig. 3(b) that the time delay increases with increasing of the amount of MWCNTs in the HA bioceramic composite. This indicates that the additives of MWCNTs lead to denser HA ceramics, decreasing its porosity [2, 6]. It is shown that the porosity of HA ceramic composite linearly depends on the time delay.

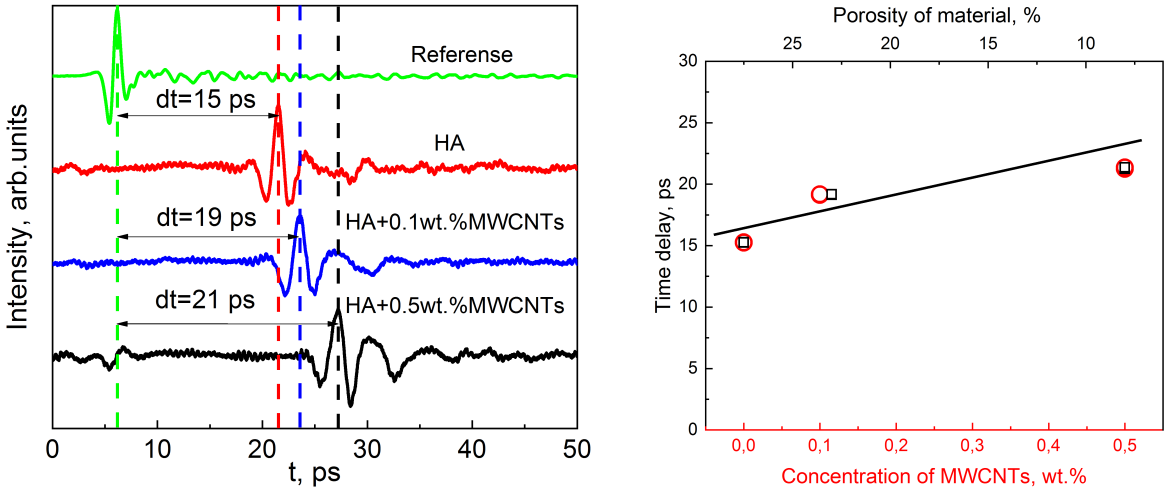

(a) (b)

FIG. 3. (a) Dependencies of the electric field strength on the time of THz pulse propagation through the air (green curve), HA ceramics (red curve), HA+0.1 wt.% MWCNTs ceramics (blue curve), HA+0.5 wt.% MWCNTs ceramics (black curve); (b) the THz pulse propagation time delay dependence on the MWCNTs concentration (open circles) and the porosity of the composite (open square). The line is mean values of the time delay.

In addition, the frequency dependencies of the refractive index (Fig. 4(a)) and absorption coefficient (Fig. 4(b)) for the studied samples are obtained. Error bars are presented standard deviation obtained from 6 measurements for each sample. The refractive index n_s and the absorption coefficient a_s in the frequency range 0.25 – 1.1 THz are obtained by using Eqs. (4) and (5), respectively. It is seen that, the absorption coefficient a_s decreases with increasing of the MWCNTs concentration up to 0.5 wt.% (Fig. 4(b)). The HA sample without nanotubes has the highest absorption coefficient, which indicates the largest porosity of the sample.

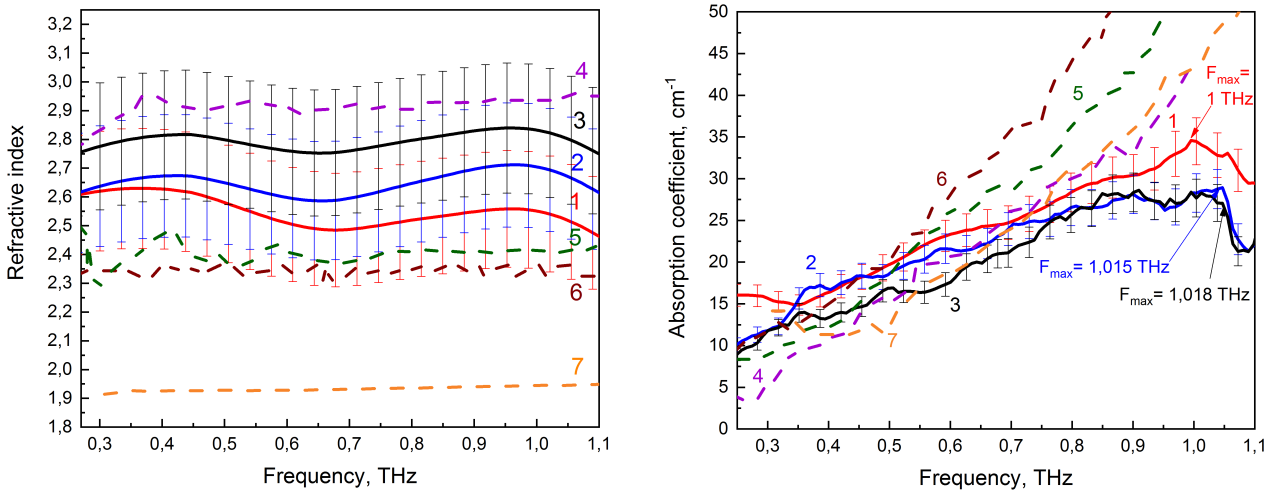

(a) (b)

FIG. 4. (a) Frequency dependence of the refractive index n: HA (solid red curve – 1), HA+0.1 wt.% MWCNTs (solid blue curve – 2), HA+0.5 wt.% MWCNTs (solid black curve – 3). Refractive indices of enamel (pink dash curve – 4), dentin [20] (green dash curve – 5), cortical human bone [14, 19] (dash brown curve – 6, dash orange curve – 7) are added for comparison; (b) Frequency dependence of the absorption coefficient a: HA (solid red curve – 1), HA+0.1 wt.% MWCNTs (solid blue curve – 2), HA+0.5 wt.% MWCNTs (solid black curve – 3). Absorption coefficients of enamel [17] (dash purple curve – 4), dentin [17] (dash green curve – 5), cortical human bone [14, 19] (dash brown curve – 6, dash orange curve – 7) were added for comparison.

The opposite effect was observed for rubber with MWCNTs additives. The absorption coefficient of rubber was increased with increasing concentration of MWCNTs, since MWCNTs are electrically conductive materials, while density and porosity of rubber were slightly changed [34, 35]. For HA composites the MWCNTs additives lead to the sintering activation and as the result, for the increase of the density and decrease of the porosity [6]. The HA ceramic sample without nanotubes additives has the highest absorption coefficient, which indicates the largest porosity of the sample. The HA sample without nanotubes has porosity ~ 27.5 %, which is ~ 3 times higher than that of the HA sample with 0.5 wt.% MWCNTs [5]. It is seen from these comparisons that the influence of MWCNTs additives to the absorption coefficient of HA and rubber are different due to the larger structural inhomogeneity of the HA composite in comparison to the rubber.

It is seen in Fig. 4(a) that the refractive indices of our ceramic samples (curves 1 – 3) indicate the same dependence in the frequency range 0.25 – 1.1 THz. It was shown that average refractive index increases from 2.6 to 2.8 with increasing of concentration of nanotubes in the HA ceramics. In different literature data of THz refractive indices for human cortical bones are as follows: $n_s \sim 1.9$ (curve 6) and 2.5 (curves 7) [14, 19]. In addition, the refractive values for enamel tissue are ~ 3.1 [17, 20, 36] and for dentin ~ 2.3 (curves 4, 5) [17, 20, 37]. The obtained results allow us to conclude that the HA with the additives of MWCNTs have the proximity of the physical properties of the ceramic material to the enamel and dentin.

In Fig. 4(b), the absorption coefficients of ceramic samples HA (curve 1) and HA-MWCNTs (curve 2 and 3) are shown. The absorption coefficients, a, obtained in our experiment (curves 1 – 3) are lower than that for cortical human bones [14, 19] (curves 6 and 7), but are close to values of absorption for enamel and dentin (curves 4 and 5) [17, 36, 37].

As for the frequency dependence of a for the HA without additives (curve 1), it shows a maximum peak at frequency $\sim$ 1 THz. For the HA with 0.1 wt.% MWCNTs (curve 2) and 0.5 wt.% MWCNTs additives (curve 3), the values of the maximum peaks are slightly shifted to higher frequency. A possible reason for this phenomenon may be an increase of noise intensity with increasing in frequency or other reasons. Plazanet et al. [38] found that the maximum peaks for pure non-stoichiometric HA is not observed in the frequency range from 0 to 2.25 THz. However, the absorption coefficient peak for the same HA heated to 1000 °C was found at frequency of 2 THz. α-TCP, β-TCP and stoichiometric (s-HA) were also observed at frequency 2.1 THz. The vibrational band is intense and narrow for s-HA [38].

It can be assumed that the position of the frequency maximum corresponds to the grain size (macrocrystallites), which increase due to recrystallization of HA ceramics during heating [38]. The diameters of macrocrystallites ($D \sim 100$ μm) were estimated by Eq. (6):

$$D = \frac{c}{fn}, \tag{6}$$

where c is the speed of light, f is the frequency, n is the refractive index.

The addition of MWCNTs leads to a small (about 10 μm) decreasing of D. In Fig. 5, the dependence of the Vickers hardness as a function of $D^{-0.5}$ was plotted by using the previous experimental the Vickers hardness values [5] and the estimated macrocrystallite sizes.

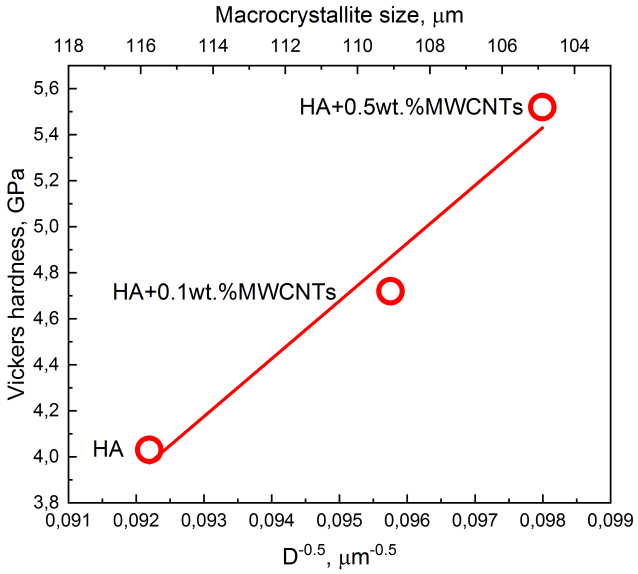

FIG. 5. Dependence the macrocrystallites sizes on the Vickers microhardness

It is seen in Fig. 5 that the hardness linearly increases with increasing concentration of nanotubes. It may be due to a decreasing in the size of macrocrystallites according to the Hall–Petch [39, 40], Eq. (7):

$$H = H_0 + k_h D^{-0.5}, \tag{7}$$

where H is the hardness, a H_0 and k_h are the material-specific constants related to hardness measurements.

We also estimate dimensionless size-parameter [41] $x \sim \pi$ by Eq. (8):

$$x = \frac{\pi D}{\lambda} = \frac{\pi D n f}{c}, \tag{8}$$

where D is the diameter of the macrocrystallites.

Previously, it was found that the X-ray diffraction peaks are slightly shifted for our samples in comparison with HA standard (JCPDS-09-0432/1996). This shift indicates the homogeneous internal macrostresses in the HA ceramics [6]. Such macrostresses can arise from the result of the low thermal diffusivity due to heterogeneous heating/cooling of the ceramics during sintering. Fig. 6 shows SEM image of agglomerates of HA powder with sizes distribution histogram. It is seen, that the average size of such macrocrystallites takes the value $D \sim 113.2$ μm. The experimental study of particles sizes corresponds to analytical calculation of the macrocrystallites sizes of HA ceramics with MWCNTs additives by using Eq. (6). A decrease in the diameters of microcrystallites in Fig. 5 is arising from the activation of the sintering process as a result of adding MWCNTs. It leads to the decrease of macrostresses between the crystallites and an increase of microhardness of the composite materials [2, 6].

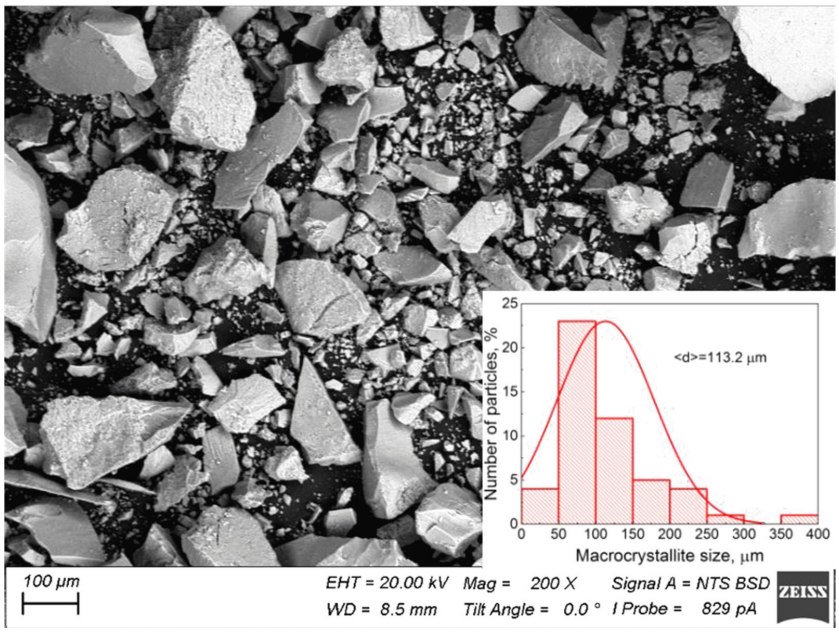

FIG. 6. SEM image of HA macrocrystallites

4. Conclusions

In this work, we used terahertz time-domain spectroscopy and optical parameters in the frequency range 0.25 – 1.1 THz to study the porous structure of a hydroxyapatite (HA) ceramics and HA ceramics reinforced with 0.1 and 0.5 wt.% multi-walled carbon nanotubes (MWCNTs). This method, based on the detection of the terahertz pulse time delay, provides information about porosity of the composites.

With an increasing in the MWCNTs concentration in the material, the time delay of the terahertz pulse propagation through the sample matrix increases. This indicates that nanotubes embedded into the HA matrix fill the pores and decrease the area of the pore space, which increases the density of the ceramic composite and decreases its porosity.

Frequency dependencies of the absorption coefficient and refractive index of HA and HA-MWCNTs ceramics were obtained for the studied samples. The obtained values show that the optical properties of the composite can be controlled by the addition of nanotubes to HA ceramics. It is shown, that with increasing concentration of nanotubes (up to 0.5 wt.%), the absorption coefficient decreases. The HA sample without MWCNTs has the highest absorption coefficient. With increasing of the MWCNTs concentration, the refractive index increases from 2.6 to 2.8, which correlates with a decrease in porosity. The values of the refractive index and the absorption coefficient of our ceramics are close to those for cortical bone, dentine and enamel. The obtained results allow us to conclude that the HA composites with additives of MWCNTs up to 0.5 wt.% have the proximity of the optical properties to the natural bone matrix.

In addition, the absorption curves show frequency peaks whose positions correspond to the grain (macrocrystallite) sizes. The size of macrocrystallites D decreases with increasing concentration of MWCNTs. This leads to an increase in the microhardness according to the Hall–Petch equation.

Thus, it was found that addition of nanotubes to ceramics makes it possible to control porosity, which affects the optical properties of the ceramic materials. This bears witness to the relation between the optical properties and porosity of the HA-MWCNTs ceramic biocomposite.

References

[1] Fiume E., Magnaterra G., Rahdar A., Verné E., Baino F. Hydroxyapatite for biomedical applications: A short overview. *Ceramics*, 2021, **4** (4), P. 542–563.

[2] Barabashko M.S., Tkachenko M.V., Neiman A.A., Ponomarev A.N., Rezvanova A.E. Variation of Vickers microhardness and compression strength of the bioceramics based on hydroxyapatite by adding the multi-walled carbon nanotubes. *Appl. Nanosci.*, 2019, **10** (8), P. 2601–2608.

[3] Han Y., Wei Q., Chang P., Hu K., Okoro O.V., Shavandi A., Nie L. Three-dimensional printing of hydroxyapatite composites for biomedical application. *Crystals*, 2021, **11** (4), 353.

[4] Ebrahimi M. Porosity parameters in biomaterial science: Definition, impact, and challenges in tissue engineering. *Front. Mater. Sci.*, 2021, **11** (4), 353.

[5] Ponomarev A.N., Barabashko M.S., Rezvanova A.E., Evtushenko E.P. Influence of Porosity on Fracture Toughness of Hydroxyapatite/Multi-Walled Carbon Nanotubes Biocomposite Materials. *Russ. Phys. J.*, 2021, **63** (11), P. 1885–1890.

[6] Barabashko M.S., Tkachenko M.V., Rezvanova A.E., Ponomarev A.N. Analysis of temperature gradients in the hydroxyapatite ceramics with the additives of multi-walled carbon nanotubes. *Russ. J. Phys. Chem.*, 2021, **95** (5), P. 1017–1022.

[7] Sreedhara S.S., Tata N.R. A novel method for measurement of porosity in nanofiber mat using pycnometer in filtration. *J. Eng. Fiber. Fabr.*, 2013, **8** (4), 155892501300800.

[8] Giesche H. Mercury porosimetry: A general (practical) overview. *Part. Part. Syst. Charact.*, 2006, **23** (1), P. 9–19.

[9] Hollamby M.J. Practical applications of small-angle neutron scattering. *Phys. Chem. Chem. Phys.*, 2013, **15** (26), P. 10566–10579.

[10] Chalmers G.R., Bustin R.M., Power I.M. Characterization of gas shale pore systems by porosimetry, pycnometry, surface area, and field emission scanning electron microscopy/transmission electron microscopy image analyses: Examples from the Barnett, Woodford, Haynesville, Marcellus, and Doig units. *Am. Assoc. Pet. Geol. Bull.*, 2012, **96** (6), P. 1099–1119.

[11] Mitchell J., Webber J., Strange J. Nuclear magnetic resonance cryoporometry. *Phys. Rep.*, 2008, **461** (1), P. 1–36.

[12] Nikoghosyan A.S., Ting H., Shen J., Martirosyan R.M., Tunyan M.Y., Papikyan A.V., Papikyan A.A. Optical properties of human jawbone and human bone substitute Cerabone® in the terahertz range. *J. Contemp. Phys.*, 2016, **51** (3), P. 256–264.

[13] Bawuah P., Markl D., Farrell D., Evans M., Portieri A., Anderson A., Goodwin D., Lucas R., Zeitler J.A. Terahertz-based porosity measurement of pharmaceutical tablets: A tutorial. *J. Infrared, Millimeter, Terahertz Waves*, 2020, **41** (4), P. 450–469.

[14] Stringer M.R., Lund D.N., Foulds A.P., Uddin A., Berry E., Miles R.E., Davies A.G. The analysis of human cortical bone by terahertz time-domain spectroscopy. *Phys. Med. Biol.*, 2005, **50** (14), P. 3211–3219.

[15] Kistenev Y.V., Nikolaev V.V., Kurochkina O.S., Borisovb A.V., Sandykova E.A., Krivova N.A., Tuchina D.K., Timoshona P.A. Use of terahertz spectroscopy for in vivo studies of lymphedema development dynamics. *Opt. Spectrosc.*, 2019, **126** (5), P. 523–529.

[16] Sudworth C.D., Fitzgerald A.J., Berry E., Zinov'ev N.N., Homer-Vanniasinkam S., Miles R.E., Chamberlain M., Smith M.A. The optical properties of human tissue at terahertz frequencies. *European Conference on Biomedical Optics*, 2003, **5143**, P. 59–68.

[17] Sim Y.C., Maeng I., Son J.-H. Frequency-dependent characteristics of terahertz radiation on the enamel and dentin of human tooth. *Curr. Appl. Phys.*, 2009, **9** (5), P. 946–949.

[18] Berry E., Fitzgerald A.J., Zinov'ev N.N., Walker G.C., Homer-Vanniasinkam S., Sudworth C.D., Miles R.E., Chamberlain J.M., Smith M.A. Optical properties of tissue measured using terahertz-pulsed imaging. *Proceedings of SPIE*, 2003, **5030**, P. 459–470.

[19] Bessou M., Chassagne B., Caumes J.-P., Pradère C., Maire P., Tondusson M., Abraham E. Three-dimensional terahertz computed tomography of human bones. *Appl. Opt.*, 2012, **51** (28), P. 6738–6744.

[20] Cai J., Guang M., Zhou J. et al. Dental caries diagnosis using terahertz spectroscopy and birefringence. *Optics Express*, 2022, **30** (8), P. 13134–13147.

[21] Zyman Z., Ivanov I., Rochmistrov D., Glushko V., Tkachenko N., Kijko S. Sintering peculiarities for hydroxyapatite with different degrees of crystallinity. *J. Biomed. Mater. Res.*, 2001, **54** (2), P. 256–263.

[22] Zyman Z.Z., Tkachenko M.V., Polevodin D.V. Preparation and characterization of biphasic calcium phosphate ceramics of desired composition. *J. Mater. Sci. Mater. Med.*, 2008, **19** (8), P. 2819–2825.

[23] Usoltseva A., Kuznetsov V., Rudina N., Moroz E., Haluska M., Roth S. Influence of catalysts' activation on their activity and selectivity in carbon nanotubes synthesis. *Phys. Stat. Sol.*, 2007, **244** (11), P. 3920–3924.

[24] Kuznetsov V.L., Krasnikov D.V., Schmakov A.N., Elumeeva K.V. In situ and ex situ time resolved study of multi-component Fe-Co oxide catalyst activation during MWNT synthesis. *Phys. Stat. Sol.*, 2012, **249** (12), P. 2390–2394.

[25] Barabashko M.S., Drozd M., Szewczyk D., Jeżowski A., Bagatskii M.I., Sumarokov V.V., Doblin A.V., Nesov S.N., Korusenko P.M., Ponomarev A.N., Geidarov V.G., Kuznetsov V.L., Moseenkov S.I., Sokolov D.V., Smirnov D.A. Calorimetric, NEXAFS and XPS studies of MWCNTs with low defectiveness. *Fullerenes, Nanotubes Carbon Nanostruct.*, 2021, **29** (5), P. 331–336.

[26] Ponomarev A., Egorushkin V., Bobenko N., Barabashko M., Rezvanova A., Belosludtseva A. On the possible nature of armchair-zigzag structure formation and heat capacity decrease in MWCNTs. *Materials*, 2022, **15** (2), 518.

[27] Kudryashov B.S., Rezvanova A.E., Ponomarev A.N., Belosludtseva A.A., Barabashko M.S. Analysis of electron microscopic images of multi-walled carbon nanotubes: Determination of the average diameter. *AIP Conference Proceedings*, 2022, **2509** (1), 020118.

[28] Barabashko M., Ponomarev A., Rezvanova A., Kuznetsov V., Moseenkov S. Young's modulus and vickers hardness of the hydroxyapatite bioceramics with a small amount of the multi-walled carbon nanotubes. *Materials*, 2022, **15** (15), 5304.

[29] TeraVil Ltd. URL: https://www.teravil.lt/t-spec.php. Accessed 27 July 2022.

[30] Nishizawa S., Sakai K., Hangyo M., Nagashima T., Takeda M.W., Tominaga K., Oka A., Tanaka K., MorikawaO. Terahertz time-domain spectroscopy. *Top. Appl. Phys.*, 2005, **97**, P. 203–270.

[31] Sakai K., Tani M. Introduction to Terahertz Pulses. *Top. Appl. Phys.*, 2006, **97**, P. 1–31.

[32] Bawuah P., Ervasti T., Tan N., Zeitler J.A., Ketolainen J., Peiponen K.-E. Noninvasive porosity measurement of biconvex tablets using terahertz pulses. *Int. J. Pharm.*, 2016, **509** (1–2), P. 439–443.

[33] Naftaly M., Tikhomirov I., Hou P., Markl D. Measuring open porosity of porous materials using THz-TDS and an index-matching medium. *Sensors*, 2020, **20** (11), 3120.

[34] Rungsawang R., Geethamma V. G., Parrott E.P.J., Ritchie D.A., Terentjev E.M. Terahertz spectroscopy of carbon nanotubes embedded in a deformable rubber. *J. Appl. Phys.*, 2008, **103** (12).

[35] Parrott E.P.J., Zeitler J.A., McGregor J., Oei Shu-Pei, Unalan H.E., Milne W.I., Tessonnier J.-P., Su Dang Sheng, Schlogl R., Gladden L.F. The use of terahertz spectroscopy as a sensitive probe in discriminating the electronic properties of structurally similar multi-walled carbon nanotubes. *Advanced Materials*, 2009, **21** (38–39), P. 3953–3957.

[36] Crawley D., Longbottom C., Wallace V.P., Cole B., Arnone D., Pepper M. Three-dimensional terahertz pulse imaging of dental tissue. *J. Biomed. Opt.*, 2003, **8** (2), P. 303–307.

[37] Nazarov M.M., Shkurinov A.P., Kuleshov E.A., Tuchin V.V. Terahertz time-domain spectroscopy of biological tissues. *Quantum Electron*, 2008, **38** (7), P. 647–654.

[38] Plazanet M., Tasseva J., Bartolini P., Taschin A., Torre R., Combes C., Rey C., Michele A.Di., Verezhak M., Gourrier A. Time-domain THz spectroscopy of the characteristics of hydroxyapatite provides a signature of heating in bone tissue. *PLoS One*, 2018, **13** (8), e0201745.

[39] Lee H.-J., Han J.-K., Janakiraman S., Ahn B., Kawasaki M., Langdon T.G. Significance of grain refinement on microstructure and mechanical properties of an Al-3% Mg alloy processed by high-pressure torsion. *J. Alloys Compd.*, 2016, **686**, P. 998–1007.

[40] Sotelo Martin L. E., Castro R. H. R. Al excess extends Hall-Petch relation in nanocrystalline zinc aluminate. *J. Am. Ceram. Soc.*, 2022, **105** (2), P. 1417–1427.

[41] Garet F., Hofman M., Meilhan J., Simoens F., Coutaz J.-L. Evidence of Mie scattering at terahertz frequencies in powder materials. *Appl. Phys. Lett.*, 2014, **105** (3), 031106.

Submitted 15 July 2023; revised 22 September 2023; accepted 23 September 2023

Information about the authors:

Anastasiya E. Rezvanova – Institute of Strength Physics and Materials Science of the Siberian Branch of the Russian Academy of Sciences, 2/4 Akademicheskii ave., Tomsk, Russia, 634055; ORCID 0000-0002-7067-7979; ranast@ispms.ru

Boris S. Kudryashov – Institute of Strength Physics and Materials Science of the Siberian Branch of the Russian Academy of Sciences, 2/4 Akademicheskii ave., Tomsk, Russia, 634055; ORCID 0009-0000-5133-4893; bsk3@ispms.ru

Alexander N. Ponomarev – Institute of Strength Physics and Materials Science of the Siberian Branch of the Russian Academy of Sciences, 2/4 Akademicheskii ave., Tomsk, Russia, 634055; ORCID 0000-0003-1524-7842; alex@ispms.ru

Anastasiya I. Knyazkova – Tomsk State University, the Faculty of Physics, 36 Lenin ave., Tomsk, Russia, 634050; ORCID 0000-0002-1454-299X; a_knyazkova@bk.ru

Victor V. Nikolaev – Tomsk State University, the Faculty of Physics, 36 Lenin ave., Tomsk, Russia, 634050; ORCID 0000-0001-8189-0188; vik-nikol@bk.ru

Yuri .V. Kistenev – Tomsk State University, the Faculty of Physics, 36 Lenin ave., Tomsk, Russia, 634050; ORCID 0000-0001-5760-1462; yuk@iao.ru

Conflict of interest: the authors declare no conflict of interest.

Authors contributions: A.E. Rezvanova, B.S. Kudryashov and A.N. Ponomarev produced ceramic porous material based on hydroxyapatite with multi-walled carbon nanotubes additives, wrote the main manuscript text and prepared all figures. A.I. Knyazkova, V.V. Nikolaev and Yu.V. Kistenev carried out THz measurements and the interpretation of the results. All authors reviewed the manuscript.

Availability of data and materials: Data underlying the results presented in this paper are not publicly available at this time but may be obtained from the authors upon reasonable request.